

## Electronic Supplementary Information

# High polarization, endurance and retention in sub-5 nm $\text{Hf}_{0.5}\text{Zr}_{0.5}\text{O}_2$ films

Jike Lyu,<sup>a</sup> Tingfeng Song,<sup>a</sup> Ignasi Fina,<sup>\*a</sup> and Florencio Sánchez<sup>\*a</sup>

<sup>a</sup> Institut de Ciència de Materials de Barcelona (ICMAB-CSIC), Campus UAB, Bellaterra 08193, Barcelona, Spain

\* ifina@icmab.es; fsanchez@icmab.es

### Contents

S1 XRD $\theta$ -2 $\theta$ scans .....	2
S2 $\chi$ -scans and pole figures .....	3
S3 Topographic AFM images .....	4
S4 Leakage current dependence on applied electric field .....	4
S5 Dependence of ferroelectric loops on maximum applied voltage .....	5
S6 PUND characterization .....	5
S7 Imprint voltage .....	6
S8 Ferroelectric retention .....	7
S9 Extended retention characterization .....	8
S10 Retention fittings and 10 years polarization extrapolation .....	8
S11 Endurance characterization and dependence on applied electric field .....	8
S12 Narrowing of the ferroelectric switching upon cycling .....	9
S13 Endurance protocol .....	10
S14 Dynamic endurance analysis .....	11
S15 Polarization switching during endurance experiments .....	11
S16 Retention protocol .....	12
S17 PUND characterization of retained polarization .....	13
References .....	13

## S1 XRD scans

Fig. S1 summarized the XRD  $\theta$ - $2\theta$  scans of all the samples.

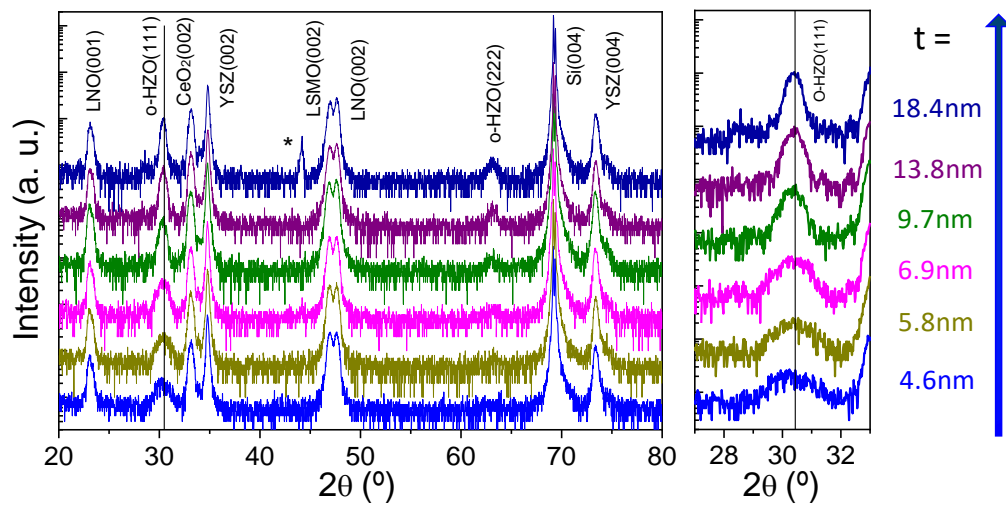


**Fig. S1:** XRD  $\theta$ - $2\theta$  scans of all the samples. The scans are vertically shifted for clarity, from the  $t = 4.6$  nm HZO film (bottom) to the  $t = 18.4$  nm film (top). The o-HZO(111) reflection is marked by the vertical line at  $2\theta = 30.4^\circ$ . The peak in the thickest film, marked by an asterisk, is a spurious reflection from silver present in the sides of the substrate. Right: zoom around the o-HZO(111) peak. Laue reflections can be appreciated in some of the scans.

## S2 $\chi$ -scans and pole figures

Fig. S2a shows the full-width at half-maximum (FWHM) as a function of the thickness of the four films shown in Fig. 1c of the manuscript. The insets show  $2\theta$ - $\chi$  frame and corresponding integration along  $2\theta$  of the representative  $t = 18.4$  nm film. Fig. S2b and S2c shows the pole figures from o-HZO(111) and Si(111) reflections of the  $t = 9.7$  nm film, confirming that the films is epitaxial and that there are four in-plane crystal variants.

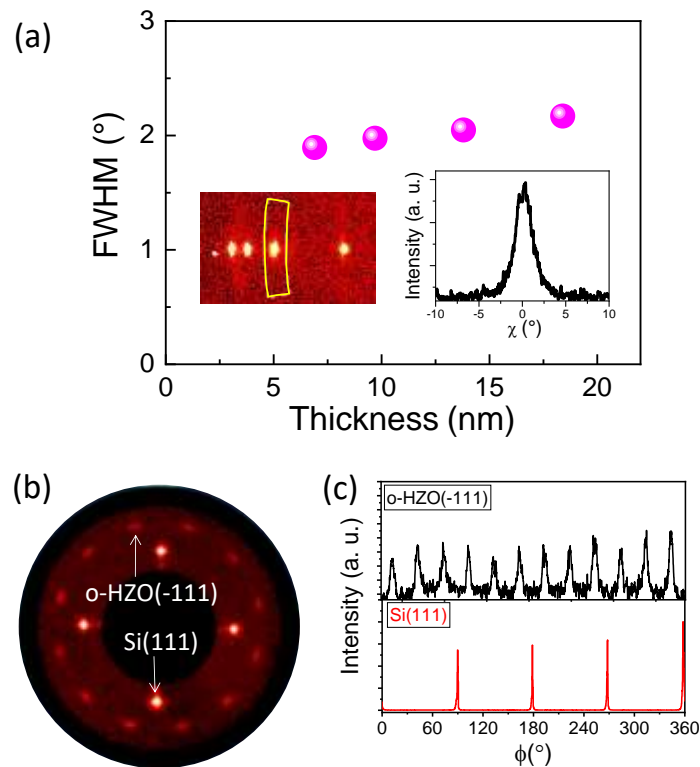


**Fig. S2:** (a) FWHM of the  $\chi$ -scans around the o-HZO(111) reflections plotted as a function of the film thickness. Left inset:  $2\theta$ - $\chi$  frame of the  $t = 18.4$  nm film and the area used for intensity integration along  $2\theta$ . The corresponding  $\chi$ -scan is in the right inset. (b) Pole figures from o-HZO(111) and Si(111) reflections of the  $t = 9.7$  nm film. (c)  $\phi$ -scans around these reflections.

### S3 Topographic AFM images

Fig. S3 shows the smooth surface of the films with low roughness slightly increasing with thickness.

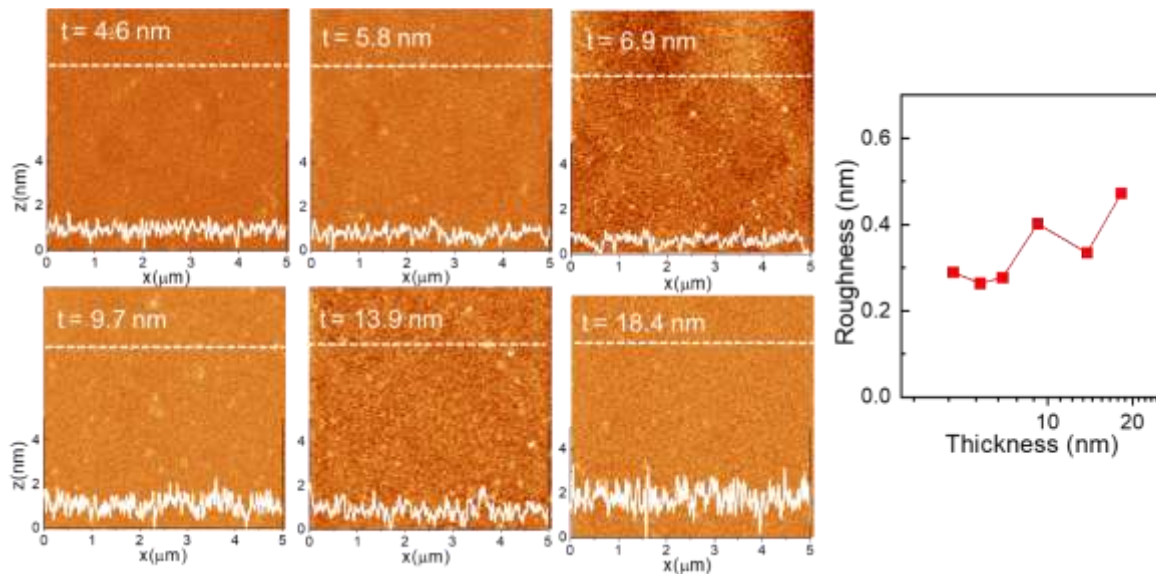


**Fig. S3:** Topographic AFM images of the films (the thickness is indicated in the top left of each image). The height profile along the dashed lines are at the bottom of each image. Bottom panel: root-mean-square rms roughness plotted as a function of the film thickness.

### S4 Leakage current dependence on applied electric field

Fig. S4 shows the decrease of leakage current of the HZO films as thickness increases.

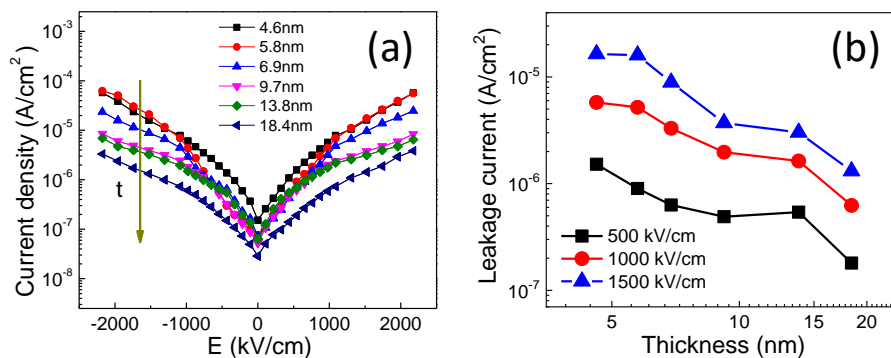


**Fig. S4:** (a) Current leakage curves of the films. (b) Leakage current at 500  $\text{kV}/\text{cm}$  (black squares), 1000  $\text{kV}/\text{cm}$  (red circles), and 1500  $\text{kV}/\text{cm}$  (blue triangles) as a function of the HZO thickness.

### S5 Dependence of ferroelectric loops on maximum applied voltage

Polarization loops measured by the DLCC method applying varying maximum voltage.

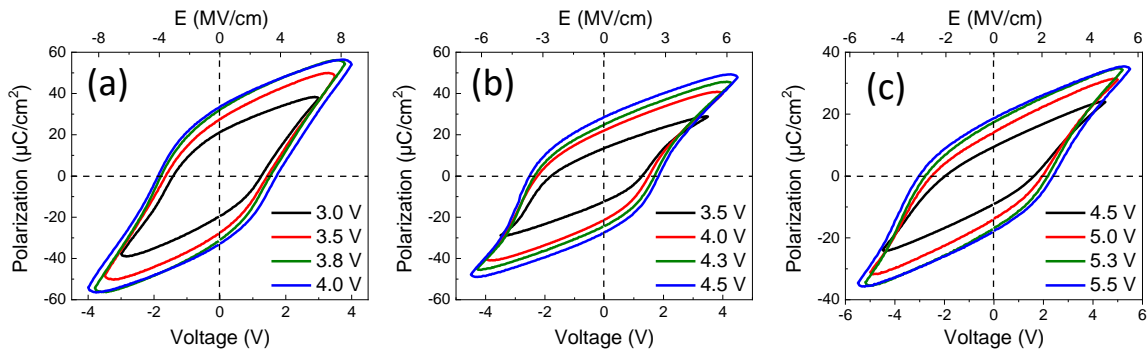


**Fig. S5:** Polarization loops of the (a)  $t = 4.6$  nm, (b)  $t = 6.9$  nm, and (c)  $t = 9.7$  nm films measured varying the maximum applied voltage.

### S6 PUND measurements

Polarization loops measured by the Positive-Up Negative-Down (PUND) method.

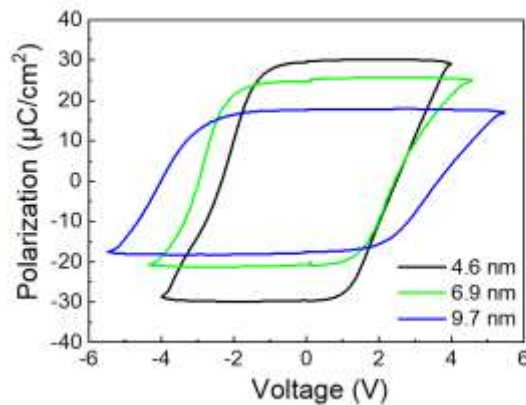


**Fig. S6:** Polarization loops of the  $t = 4.6$  nm, 6.9 nm, and 9.7 nm films measured by the PUND method using delay time between pulses of 1s. Loops displayed here show larger coercive field compared to those shown in Figure 2 of the main text due to the so-called fluid imprint field.<sup>S1</sup> Therefore, fully saturated loops can not be obtained and polarization is underestimated using PUND technique.

### S7 Imprint voltage

$V_{\text{imp}}$  dependence on thickness shows an abrupt increase up to 6.9 nm. Above this thickness  $V_{\text{imp}}$  saturates around 0.35 V.

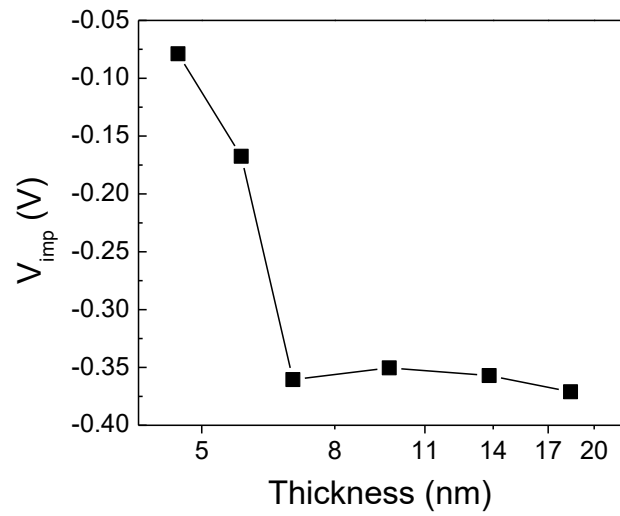


**Fig. S7:** Imprint voltage ( $V_{\text{imp}}$ ) as a function of the HZO thickness.

## S8 Ferroelectric retention

Fig. S8(a-f) show the  $P_r$  dependence on time for all the films

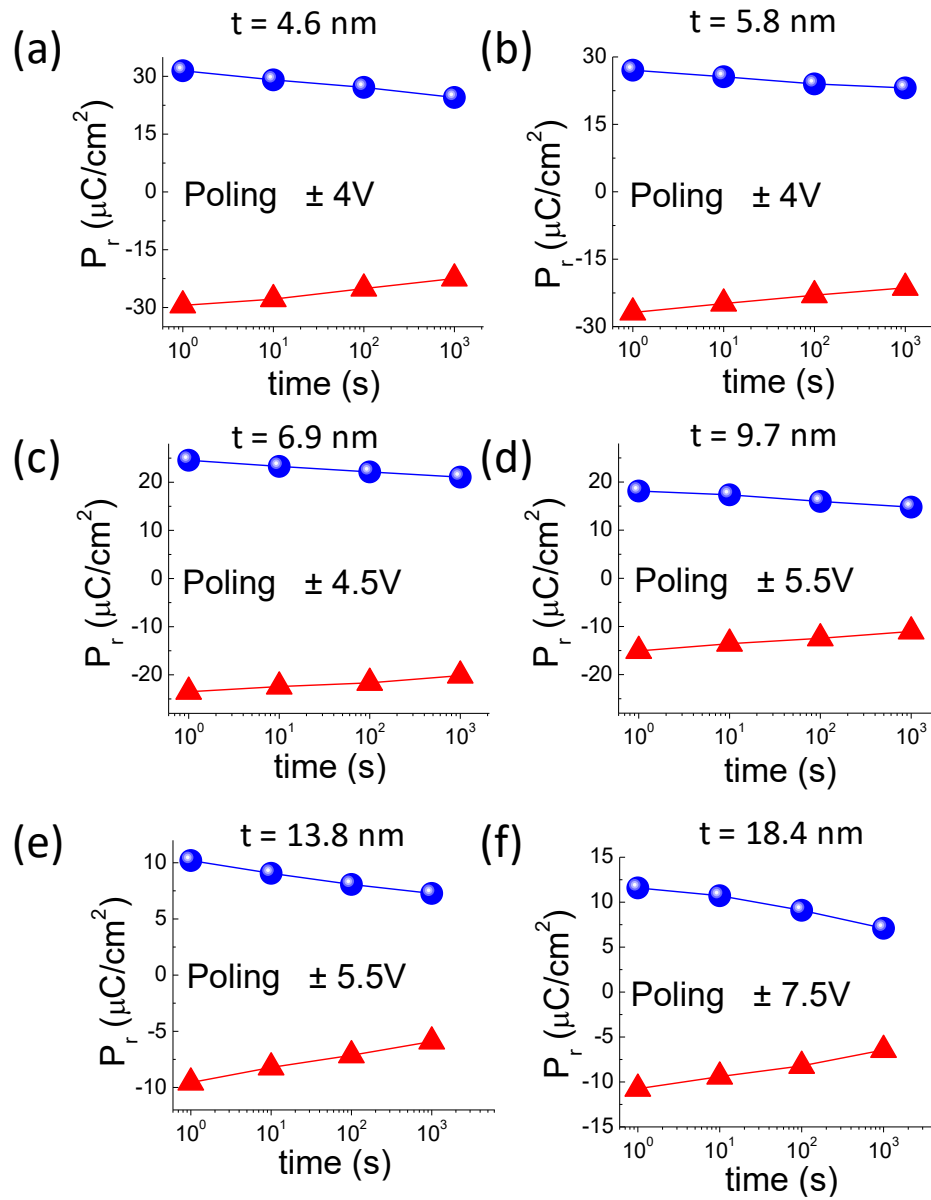


**Fig. S8.** Polarization retention after positive (blue circles) and negative (red triangles) poling.

### S9 Extended retention characterization

Retention measurements extended to  $10^4$  seconds and/or after poling at varying voltage.

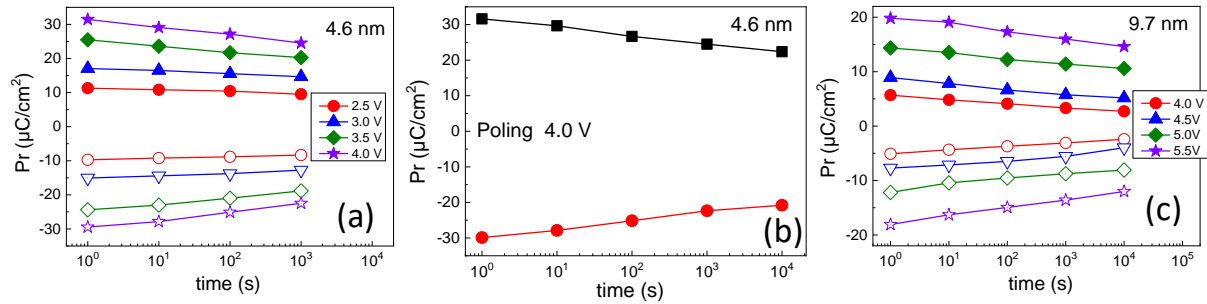


**Fig. S9.** Retention measurements of the  $t = 4.6$  nm film (a) after poling at varying voltages, (b) up to  $10^4$  s after poling at 4.0 V. (c) Retention measurements of the  $t = 9.7$  nm film up to  $10^4$  s after poling at varying voltages.

### S10 Retention fittings and 10 years polarization extrapolation

Fig. S10 shows the  $P_r$  dependence on time and the data fitting using the rational relation  $P_r = P_0 t^{-k}$ . Data fitting allows to infer that  $P_r$  is safely above detection level after 10 years for the 6.9 nm film and thinner.

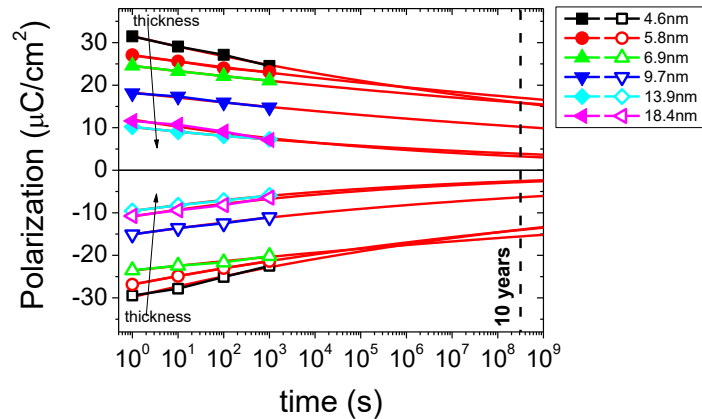


**Fig. S10.** Polarization retention after positive (blue circles) and negative (red triangles) poling and corresponding fitting.

### S11 Endurance characterization and dependence on applied electric field

The plot of the normalized remnant polarization of all the samples as a function of the number of cycles summarizes the impact of thickness on ferroelectric fatigue (Fig. S11a). We note that the voltage used for poling each sample determines when the breakdown occurs, but it only smoothly affects the normalized polarization. The reduction of polarization when the thinnest

films are cycled is not abrupt, and the  $t = 4.6$  nm film retains more than 70% of the initial remnant polarization after  $10^6$  cycles. In contrast, the remnant polarization of the  $t = 18.4$  nm film is less than 15% after the same number of cycles. Fig. S11b maps the endurance as a function of the electric field. Measurements ended with hard breakdown of the capacitor (empty symbols), or were stopped when the memory window was below  $2 \mu\text{C}/\text{cm}^2$  or after  $10^{11}$  cycles (solid symbols). Fig. S11 demonstrates the huge impact of thickness on the endurance, and the robustness of the ultrathin epitaxial HZO films against fatigue.

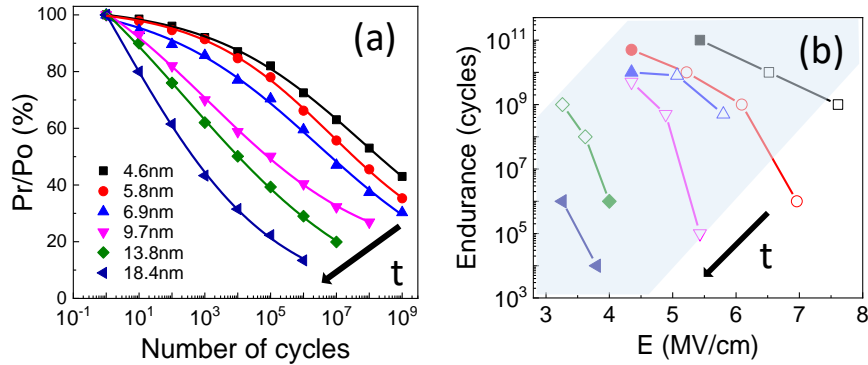


**Fig. S11.** (a) Endurance of the films, being the polarization normalized to the value of the pristine state of each film. (b) Endurance as a function of the poling electric field. Symbols corresponding to the different samples are in the inset of (a). Empty symbols indicates hard breakdown.

### S12 Narrowing of the ferroelectric switching upon cycling

The J versus voltage curves corresponding to the P-V loops of Fig. 4d are shown in Fig. S12a. It can be observed that the ferroelectric switching peaks are well-visible. Near the maximum applied voltage, the series resistance (encircled by solid line) and some residual leakage current contribution (encircled by dashed line) are present producing the round shape of the P-V loops near the maximum applied voltage. Note that the residual leakage contribution decreases with the number of cycles. Note also that these measurements are performed using DLCC and thus there is not relation between the leakage current plotted in Fig. 4e and the residual leakage observed here. Also, it is important the change on the broadness of the ferroelectric switching upon cycling. In Fig. S12a, it can be observed that while for the pristine loop the ferroelectric switching peak is broad and one can distinguish the presence of two contributions, for the cycled loops the ferroelectric switching peak is abrupt. This fact can be related to reminiscent wake-up effect without important change in the polarization value measured. The effect of the narrower switching peak with cycling can be observed in Fig. S12b,c. In Fig. S12b, the J versus

voltage loop has been simulated for different broadness of the ferroelectric switching ( $\Delta E_c = \Delta E_c^*$ ,  $3/4 \cdot \Delta E_c^*$  and  $1/2 \cdot \Delta E_c^*$ ) peak all having the same saturated polarization following the expressions described in ref. S2. The extracted P-V loop shown for  $\Delta E_c^*$  in Fig. S12c is more round shaped near the maximum applied voltage due to the mentioned broadening.

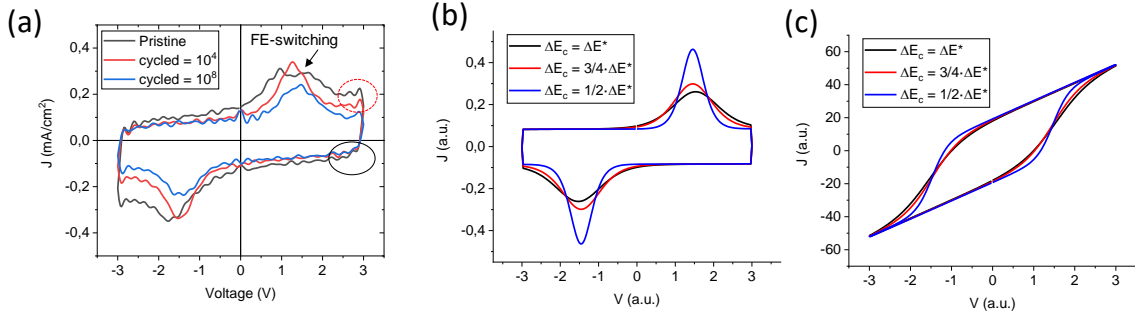


**Fig. S12.** (a)  $J$  versus voltage loops of the corresponding P-V loops shown in Figure 4d. (b) Simulated J-V loops using different indicated coercive field broadness ( $\Delta E_c$ ) according to reference.<sup>S2</sup> (c) P-V loop extracted from panel b. It can be observed that the remarkable difference between the J-V loops of panel (b), difference in the shape of the P-V loops shown in panel (c) is not so visible. Similar observation can be done comparing the J-V loops of panel (a) with the P-V loops of Figure 4d of the main text.

### S13 Endurance protocol

The endurance has been evaluated using bipolar square pulses with cycling frequency of 100 kHz. The polarization and the imprint electric field after the indicated number of cycles has been measured at 1 kHz and applying bipolar triangular pulses using the DLCC method.<sup>S3</sup> In Fig. S13, we show a scheme of the used protocol. The leakage endurance (Figure 4e in the manuscript) has been determined by performing a I-V characteristics measurement up to 3.5 V, instead of measuring a P-V loop, and extracting the leakage current at the indicated applied voltage.

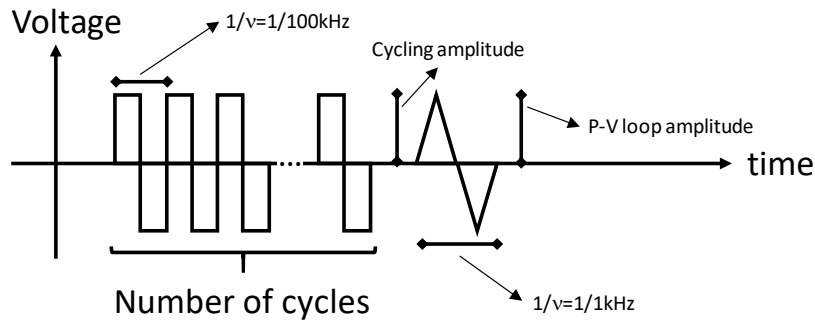


**Fig. S13.** Scheme of the voltage pulse train used to perform the endurance characterization. The bipolar triangular pulses used to determine the loop has been simplified for easy understanding. The actual bipolar triangular pulses are described in refs.<sup>S3,S4</sup>

### S14 Dynamic endurance analysis

The dependence of the fatigue measured at 4.5 V and cycling frequencies varying from 1 kHz to 100 kHz, for the  $t = 9.7$  nm film, is plotted in Fig. S14. At 1 kHz, equivalent to a 0.5 ms pulse width, switching time must be fast enough to allow polarization switching as inferred from the loops measured at the same frequency shown in Figure 2a of the manuscript. In Fig. S14, it can be observed that while cycling frequency is increased the measured polarization is similar. In particular, at 100 kHz, which is the cycling frequency shown in all the fatigue experiments shown in the main manuscript, no variation is observed. Therefore, it can be concluded that the switching dynamics does not play a relevant role in the endurance experiments displayed.

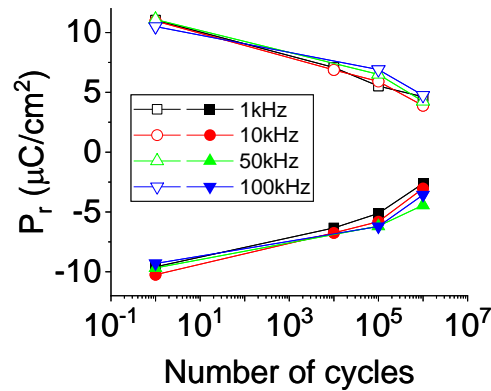


**Fig. S14.** Endurance of the  $t = 9.7$  nm film, measured at 4.5 V and cycling frequencies varying from 1 kHz to 100 kHz.

### S15 Polarization switching during endurance experiments

We performed experiments related to the polarization switching dynamics during the endurance experiments for the 4.6 nm film, and these are summarized in Fig. S15. In Fig. S15, we plot PU experiments after negative prepoling using square pulses, as during the endurance experiments. In PU experiments, the polarization integrated during the first P pulse results from leakage and polarization switching contributions. The second pulse accounts only for the leakage. Therefore, the difference between polarization integrated during P and U accounts for the switched polarization ( $2 \cdot P_r$ ) indicated in red in the figures. Fig. S15a has been collected using 1 kHz equivalent frequency for the square pulses, and obtaining  $P_r = 30.5 \mu\text{C}/\text{cm}^2$ . Note that this polarization value is somehow smaller than the value obtained in the P-V loops measured at 3.0 V (Fig. S5a) due to the influence of the fluid imprint field in PUND characterization (as explained in the text). Fig. S15b,c show similar experiments at 10 and 100 kHz, respectively, being 100 kHz the frequency used in the endurance measurements shown in the main text. It

can be observed that the switched polarization gradually decreases. For 100 kHz this decrease is around 5 %. Thus, the performed detailed analysis allow us to conclude that polarization is not completely switched during the endurance experiments. However, the partial switching is small ( $\approx 5\%$ ) and, as revealed by Fig. S14, without impact in the endurance characterization. The performed experiments show that partial polarizations switching starts between the 10 - 100 ms pulse width range. Thus, the partial polarization is most probably limited by the time constant of our experimental set-up, rather than the intrinsic ferroelectric switching dynamics, which is expected to be faster.

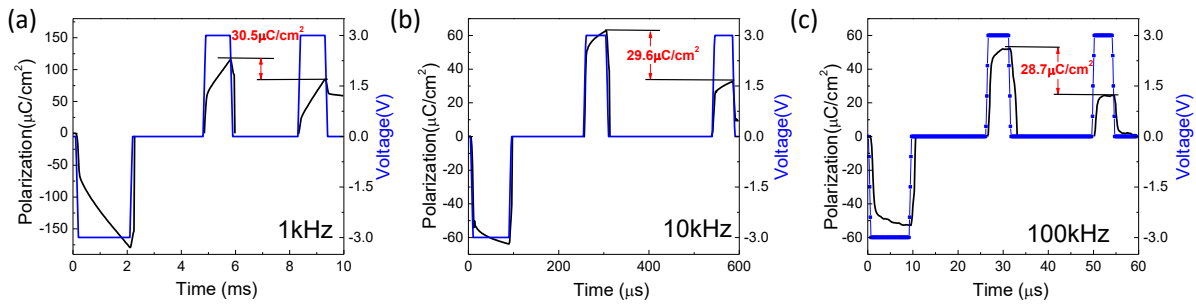


**Fig. S15.** PU experiments after negative prepoling using square pulses of equivalent (a) 1 kHz, (b) 10 kHz and (c) 100 kHz frequencies.

### S16 Retention protocol

Retention measurements were done using long enough (0.25 ms) triangular prepolarizing pulse (positive or negative) to ensure polarization saturation. Afterwards, ND and or PU pulses were applied to define the remnant polarization state for positive or negative prepolarizing voltages, respectively (see Fig. S16). PUND pulses frequency was 1 kHz corresponding to the frequency at which ferroelectric hysteresis loops were recorded.

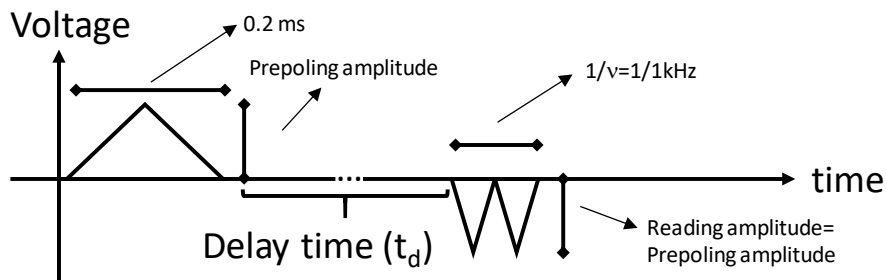


**Fig. S16.** Positive voltage prepoled polarization scheme. For negative voltage prepolarizing inverted signs in all pulses are used.

### S17 PUND characterization of retained polarization

In Fig. S17b, the polarization curves after subtraction resulting from the selective ND and PU pulse measurements are shown. It can be observed that the polarization values are obtained from well-saturated curves. Note that the loops are open due to the PUND method only accounts for switchable polarization and this is asymmetric. In Fig. S17a, the polarization retention experiment displayed in Electronic Supplementary Information S8, which data is also shown in Figure 3 of the manuscript, is plotted for comparison. Thus, as far as, the measurement conditions in retention experiments are “slow” switching dynamics can not importantly affect the obtained results.

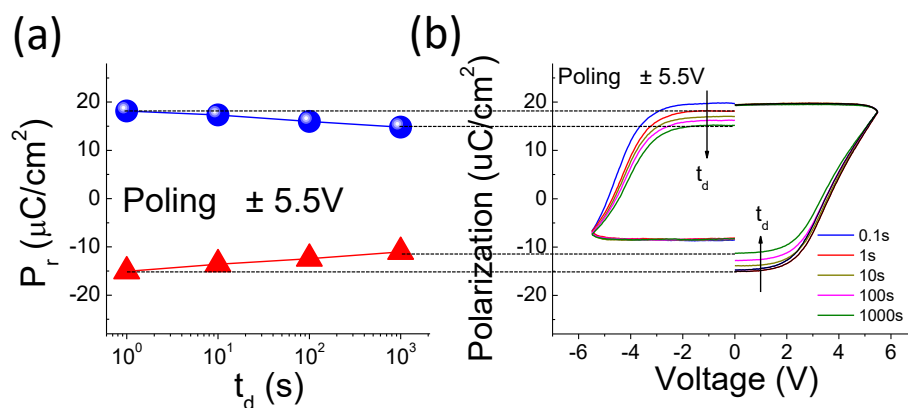


**Fig. S17.** (a) Polarization retention after positive (blue circles) and negative (red triangles) poling for 9.7 sample. (b) Polarization versus voltage semi-loops after subtraction resulting from the selective ND and PU pulse measurements.

### References

- <sup>S1</sup> P. Buragohain, A. Erickson, P. Kariuki, T. Mittmann, C. Richter, P. D. Lomenzo, H. Lu, T. Schenk, T. Mikolajick, U. Schroeder, and A. Gruverman, *ACS Appl. Mater. Interf.*, 2019, **11**, 35115.
- <sup>S2</sup> S. González-Casals, I. Fina, F. Sánchez, J. Fontcuberta, *ACS Appl. Electron. Mater.*, 2019, **1**, 1937.
- <sup>S3</sup> I. Fina, L. Fàbrega, E. Langenberg, X. Martí, F. Sánchez, M. Varela, and J. Fontcuberta, *J. Appl. Phys.*, 2011, **109**, 074105.
- <sup>S4</sup> R. Meyer, R. Waser, K. Prume, T. Schmitz, and S. Tiedke, *Appl. Phys. Lett.*, 2005, **86**, 142907.